Joining YSZ electrolyte to AISI 441 interconnect for solid oxide cells using the Ag interlayer: Enhanced mechanical and aging properties

Xiaoqing Si
Harbin Institute of Technology
Xiaoyang Wang
Harbin Institute of Technology
Chun Li
Harbin Institute of Technology
Tong Lin
Harbin Institute of Technology
Junlei Qi
Harbin Institute of Technology
Jian Cao (cao_jian@hit.edu.cn)
Harbin Institute of Technology https://orcid.org/0000-0002-9159-7943

Research Article

Keywords: Solid oxide fuel/electrolysis cells, Diffusion bonding, YSZ, Pure Ag interlayer, Aging

Posted Date: July 23rd, 2021

DOI: https://doi.org/10.21203/rs.3.rs-738261/v1

Abstract

Conventional Ag-CuO braze can lead to two electrolyte/interconnect joining issues: over-oxidation at the steel interconnect and hydrogen-induced decomposition of CuO. This work demonstrates that a pure Ag interlayer, instead of Ag-CuO braze, can join YSZ electrolyte to AISI 441 interconnect in air. Reliable joining between YSZ and AISI 441 can be realized at 920 °C. A dense and thin oxide layer (~2 μm) is formed at the AISI 441 interface. Also, an interatomic joining at the YSZ/Ag interface is detected by TEM observation. Obtained joints display high shear strengths (~86.1 MPa), 161% higher than that of joints brazed by Ag-CuO braze (~33 MPa). After aging in reducing and oxidizing atmospheres (800 °C/300 h), joints remain tight and dense, indicating a better aging performance. This technique eliminates the CuO-induced issues, which will extend lifetimes for SOFC/SOEC stacks and other ceramic/metal joining applications.

1. Introduction

As electrochemical conversion devices, solid oxide fuel/electrolysis cells (SOFC/SOEC) are increasingly widely applied in practice due to high efficiency, fuel diversity, and ultra-low pollution [1–5]. Yttria-stabilized zirconia (YSZ) ceramics, possessing excellent fracture toughness, chemical stability, and high ionic conductivity at elevated temperatures, have become the most successful and commonly used electrolyte for SOFCs/SOECs [6–9]. Typically, single cells are combined into SOFC/SOEC stacks to obtain sufficiently high voltage [10, 11]. To date, the planar SOFC/SOEC design achieves the broadest applications owing to its easy stacking characteristics [12–14]. The most critical process in fabricating the planar stack is the sealing between solid oxide cells and ferritic stainless steel interconnects. And as-sealed joints are required to be stable during the subsequent long-term high-temperature service [15, 16].

Glass/glass-ceramic bonding and reactive air brazing (RAB) are currently two promising methods to join cells to interconnects [17–19]. For the glass/glass-ceramic materials, their composition can be tailored to match the thermomechanical requirements of the SOFC/SOEC stack components [20, 21]. But problems, like the crystallization during sintering/operation and inherent brittleness of the glass-based sealants, may be detrimental to the long-term stability of joints [22, 23]. Fortunately, RAB is an alternative technique to satisfy the sealing requirements without the above issues. This method can be performed directly in air with a noble metal (Ag, Pt, Au, Pd) -oxide (CuO, V_2O_5, Nb_2O_5, SiO_2) braze system [24–26]. The oxide modifies or reacts with the substrate surface, thus promoting the wetting behavior of the braze on the newly formed surface [27, 28]. Up to now, the Ag-CuO is the most effective and commonly used RAB braze for joining SOFC/SOEC components [29–31].

However, recent studies have pointed out that the introduction of CuO can give rise to two major issues. One is the thick and loose Cu/Cr/Mn/Fe-oxide layer (typically ≥ 20 μm) at the braze/interconnect interface due to the reaction between the CuO from the braze and the steel interconnect [25, 32, 33]. Moreover, the rapid growth of this oxide layer is proved to be a key factor for the RAB joint failure during aging [17]. The other issue for the Ag-CuO braze is that CuO is thermodynamically unstable when

exposed to the reducing atmosphere in fuel (i.e., anode) chambers [7, 31]. The decomposition of CuO through the reaction $CuO + H_2 \rightarrow Cu + H_2O$ and the subsequent solid solution of Cu into the Ag matrix can lead to many voids [4, 34]. Besides, these voids can offer rapid paths for hydrogen permeation into the joint central region (where the hydrogen reacts with diffused oxygen to generate gaseous water pockets), consequently weakening the gas-tightness and mechanical properties of joints [31, 35–37]. However, it is noted that the joints mainly composed of Ag with good plasticity still have an irreplaceable role when the SOFC/SOEC stack is used as a mobile device [38, 39].

A sealant without the CuO should be tested to solve the problems caused by the CuO-containing braze, and a pure Ag interlayer might be a good choice. Considering the liquid Ag can only wet the YSZ electrolyte to a limited extent, which is not enough to provide a sufficient joining for the YSZ-electrolyte/steel-interconnect structure in the SOFC/SOEC stack. Therefore, this work intends to apply the pure Ag interlayer to replace the Ag-CuO braze for joining the YSZ electrolyte and AISI 441 interconnect below the melting point of Ag. The benefits of this approach are apparent. (□) The oxide layer at the interconnect interface can be effectively mitigated due to the absence of CuO. (□) The decomposition of CuO and the consequent damage to the joint stability are entirely avoided. (□) The overflow of braze in traditional braze methods (such as vacuum brazing, glass/glass-ceramic bonding, RAB, etc.) can be solved. However, whether a high-strength joining between the YSZ-electrolyte and steel-interconnect can be achieved without the CuO modification is unclear. Besides, the aging performance of joints should also be studied in detail.

In this study, the YSZ electrolyte is joined to the AISI 441 interconnect using a pure Ag interlayer directly in air. The microstructure, forming mechanism, mechanical properties, and the effects of bonding temperature on the joint are in-depth studied. Besides, the long-term stability of joints both in oxidizing and reducing atmospheres is evaluated.

2. Experimental Procedures

2.1 Materials

The YSZ electrolyte (containing 3 mol% yttria) adopted in this work is purchased from Shanghai Unite Technology Co., Ltd. AISI 441 stainless steel (a kind of ferritic stainless steel) to be joined is obtained from Baowu Iron and Steel Group Co., Ltd, China, with a thickness of ~ 2 mm. And its composition is displayed in Table 1. Ag powder (Aladdin, 99.95%, ≤ 10 μm) was pressed (100 MPa, 180 s) into a ~ 100-μm-thick tablet via a tableting instrument. The morphology of Ag powder can be seen in the supplementary material (Fig. S1).

Table 1
Composition of the AISI 441 stainless steel (wt.%).

	Cr	Mn	Si	Nb	Ti	Al	Fe
content	17.53	0.40	0.59	0.41	0.17	0.07	balance

2.2 Joining process

Before joining, AISI 441 stainless steel is cut into 10 × 10 × 2 mm^3 pieces using a wire electric discharge machine and subsequently polished with a 1200 # abrasive paper. YSZ ceramics are cut into 5 ×5 × 3 mm^3 specimens using a diamond wire saw. Then both the AISI 441 pieces and YSZ specimens are ultrasonically cleaned in ethanol for 20 min. The Ag tablet was sandwiched between the YSZ and AISI 441. Meanwhile, a pressure (~ 2 MPa) is put on the top of the sandwich to ensure tight contact during joining, as shown in Fig. 1a. Finally, these assemblies are sintered in a muffle furnace (KSL-1400X) and heated at a series of temperatures (890–970℃) for 30 min (see temperature curve in Fig. 1c).

2.3 Long-term tests in reducing and oxidizing atmospheres

Two groups of tests are conducted to assess the long-term stability of the joints in reducing and oxidizing atmospheres. In both tests, the obtained joints are placed in an alumina crucible and exposed in a horizontal tube furnace (OTF-1200X) and heated at 800 ℃ for 300 h (heating and cooling rates of 5 ℃/min). To simulate the reducing atmosphere in the fuel chamber, the compressed gas (5%H_2, 95% Ar) is flown through a water container (heated to 80 ℃ for 50% humidity) to obtain a wet reducing atmosphere containing 50% (H_2 + Ar) and 50% H_2O. Meanwhile, the gas flow is kept at 6 L/h. As for the aging test in the oxidizing atmosphere, the compressed air is flown into the above horizontal tube furnace, with a constant gas flow of 6 L/h.

2.4 Microstructural characterization and shear test

To observe the microstructure of the YSZ/AISI 441 joints, scanning electron microscopy (SEM, Quanta 200FEG, America) combined with an energy dispersive spectrometer (EDS) is adopted. For further analysis at the YSZ/Ag interface, a focused ion beam (FIB, Helios Nano Lab 600i, America) is used to prepare the sample with a thickness of 50–100 nm. Subsequently, this sample is detected by a transmission electron microscope (TEM, Talos F200X, America).

A universal mechanical testing machine (Instron 1186, America) is used to measure the shear strength of the joint. The schematic illustration of the shear test is depicted in Fig. 1b. Five samples are measured and averaged at each temperature.

3. Results And Discussion

3.1 Interfacial microstructure of YSZ/AISI 441 joint

Figure 1a displays the overall SEM image of the YSZ/AISI 441 joint obtained with the pure Ag interlayer at 920 ℃/30 min in air. It is apparent that a tight joint is formed under this condition. Both the YSZ/Ag interface and the AISI 441/Ag interface seem compact and defect-free. The corresponding enlarged SEM images (Fig. $2a_1$ and $2a_2$) are obtained for further details about these two interfaces.

A thin and dense oxide layer (~ 2 μm) is formed between Ag and AISI 441 (Fig. $2a_2$), which has been proved to be composed of (Fe, Mn, Cr)$_3O_4$ and Cr_2O_3 by many studies [25, 40–42]. It is worth noting that the oxide layer formed at the stainless steel interface by the traditional RAB method is typically thicker than 20 μm [25, 32, 33], which is 10 times wider than the above oxide layer. The dramatic reduction of the oxidation layer thickness is due to the absence of CuO and the lower joining temperature (920°C, while the traditional RAB method generally requires temperatures higher than 970°C). Besides, compared with ≥ 20μm thick oxide layer, this thin oxidation layer may help maintain the long-term stability of the joint.

It can be seen from the enlarged view in Fig. $2a_1$ that the YSZ/Ag interface is still dense without micro-voids or micro-cracks. It is well documented that a tight atomic bonding is essential to fabricate a stable joint [43], while it is hard to judge whether there is atomic bonding between YSZ and Ag only by SEM. Therefore TEM is adopted to further analyze the YSZ/Ag interface. Figure 2b exhibits the bright-field image at the YSZ/Ag interface, and the corresponding elemental distribution (Zr and Ag) is shown in Fig. 2c.

The element distribution indicates that Ag and YSZ are closely joined without apparent gaps. The enlarged view in Fig. $2c_1$ reveals that a small number of Ag atoms diffuse into the YSZ, forming a diffusion layer with a width of ~ 3 nm. As shown in Fig. 2d, the elemental distributions of Ag, Zr, and O along the yellow line in Fig. 2b also indicate that a diffusion layer (~ 3 nm) exists between Ag and YSZ. This diffusion phenomenon might play a crucial role in forming a hermetic joint. High resolution transmission electron microscope (HRTEM) is used to determine the bonding type between YSZ and Ag. The HRTEM image in Fig. 2e depicts that the crystal lattices of Ag and YSZ are clearly visible. The enlarged view (Fig. $2e_1$) of region 4 and the corresponding Fast Fourier Transformation (FFT) (Fig. $2e_2$ and $2e_3$) note that the [220] zone axis of the ZrO_2 is paralleled to the [0—11] axis of the Ag. In addition, a disordered lattice region (~ 3 nm) is observed between Ag and YSZ, which might attribute to the diffusion of Ag into the YSZ. The above TEM analysis demonstrates that atomic bonding is achieved between YSZ and Ag, which is the premise of obtaining an airtight joint with superior mechanical properties.

3.2 Effect of bonding temperature on YSZ/AISI 441 joint

Since the joining temperature is an essential factor affecting the microstructure and properties of the joint, the microstructures of the joints obtained at various joining temperatures (860–970 ℃) for 30 min are observed in this section as displayed in Fig. 3.

It can be seen from Fig. 3a-3d that tight and well-formed joints can be obtained at the temperature of 860–970 ℃. Fine and dense bonding is formed at both the YSZ/Ag interface and AISI 441/Ag interface.

At these temperatures, no defects or voids are observed at the YSZ/Ag interface. This may be because Ag is soft enough to fill the gaps at this interface under the pressure of ~ 2 MPa. In addition, since there is no reaction product between Ag and YSZ, and both are stable at 860–950 ℃, no noticeable change of the interfacial microstructure at various temperatures can be observed via the SEM method (the enlarged SEM image of YSZ/Ag interface is not shown).

For the AISI 441/Ag interface (see Fig. $3a_1$-$3d_1$), the oxidation behavior is intensified with elevating temperatures. At 860°C (Fig. a_1), a discontinuous oxide is formed at the AISI 441 interface. The oxide layer is thickened with the increasing temperature, and a continuous and dense oxide layer (2–3 μm in thickness) is observed at 950°C (Fig. d_1).

In addition, when the temperature reaches 970 ℃ (higher than the melting point of Ag), the joint quality decreases significantly,which can be seen in the supplementary material (Fig. S2). Most of the Ag flows away from the gap between YSZ and AISI 441, and only a slight residual Ag exists between YSZ and AISI 441. This phenomenon can be attributed to the high contact angle of pure Ag on the YSZ surface and no reaction between YSZ and Ag, resulting in the loss of liquid Ag during joining [34, 44].

3.3 Shear strength of joints at various bonding temperatures

Shear strength is an essential indicator for measuring joint quality, so shear tests are conducted for the joints obtained at different temperatures in this section. Subsequently, the fracture surfaces after shear tests are analyzed by SEM to understand the failure mechanism further.

Figure 4a notes that the shear strength of the joint first increases and then decreases with the increasing temperature (from 860 ℃ to 970 ℃), reaching the maximum (86.1 MPa) at 920 ℃. Figure 4b illustrates the AISI 441-side fracture morphology of the joints obtained at 860°C. The fracture mainly occurs between YSZ and Ag, and no noticeable dimple on the Ag surface is observed. This phenomenon indicates a poor bonding strength between Ag and YSZ at 860°C, owing to insufficient diffusion between Ag and YSZ at lower temperatures. Hence the joints exhibit low shear strength at low temperatures (20.1 MPa at 860°C). When the joining temperature increases to 890°C, the shear strength is significantly increased to 64.6 MPa. As shown in Fig. 4c, part of the fracture begins to occur between Ag and AISI 441. On the one hand, this is due to the increase of the YSZ/Ag interfacial strength as the temperature rises. On the other hand, the thickening of the oxide layer on the AISI 441 surface may reduce the bonding strength at the AISI 441/Ag interface. The maximum shear strength is reached at 920°C. The fracture occurs at both the YSZ/Ag interface and the AISI 441/Ag interface (see Fig. 4d). Besides, many dimples are observed at the Ag layer, indicating a large plastic deformation and high strength at YSZ/Ag interface. A further increase in temperature will reduce the joint strength (55.8 MPa at 950°C), mainly due to the increased oxidation of the AISI 441 surface, as shown in the enlarged view of area 8. In addition, when the joining temperature rises to 970 ℃ (exceeding the melting point of Ag), the shear strength drops sharply to 2.5 MPa. The reason has been explained in detail in Sect. 3.2.

According to the research of Cao et al. [25], the shear strength of the YSZ/AISI 441 joint obtained using traditional Ag-CuO braze at 960 ℃/30 min is ~ 33 MPa. Surprisingly, the joint strength in this study can reach 86.1 MPa, which is 161% higher than that of traditional RAB joints. The significant enhancement in shear strength could be explained by the lower joining temperature (920°C) that reduces the oxidation at the AISI 441 surface. Meanwhile, the absence of CuO further alleviates the oxidation of the metal surface.

3.4 Stability of joints in reducing and oxidizing atmospheres

To assess the long-term stability of the joints in SOFC/SOEC relevant atmospheres, the YSZ/441 joints obtained with pure Ag interlayer at 920 ℃/30 min were aged for 300 h at 800°C in 50% (H_2 + Ar)-50% H_2O and air atmospheres, respectively. And the aging results are analyzed as follows.

Figure 5 presents the cross-sectional SEM images of the joints after exposure in 50% (H_2 + Ar)-50% H_2O at 800 ℃ for 300 h. Obviously, aging for 300 h in the reducing atmosphere does not cause any significant change in the overall morphology of the joint. No defects (such as delamination, cracks, or voids) due to reduction are observed. The enlarged views of the two interfaces are subsequently observed for further details. It can be seen from Fig. 5a_1-c_1 that the YSZ/Ag interface remains compact and well bonded, and the reducing atmosphere has no apparent effect on this interface. The good reduction resistance of the interface may be attributed to the Ag-ZrO_2 atomic bonding. The AISI 441/Ag interface also shows excellent stability in reducing atmosphere at 800 ℃, as shown in Fig. 5a_2-c_2. The oxide layer at the AISI 441 interface remains compact, and its thickness does not seem to change after exposure to reducing atmosphere for 300 h. This may be because the oxide layer is thermodynamically stable under this condition and is difficult to be decomposed by reduction. Notably, the voids caused by the CuO reduction, which is inevitable in the traditional RAB method [4, 31, 34, 37], are completely eliminated.

Figure 6 displays the joint structure after aging in air at 800 ℃ for 300 h. It can be seen from the low-magnification SEM images in Fig. 6a-6c that the joints maintain tight bonding in a wide range without delamination after oxidation for 300 h. Besides, the oxide layer on the AISI 441 surface is thickened with the increasing oxidation time. Also, no apparent defects are observed in cross-sectional SEM images from Fig. 6a_1-6c_1. The YSZ/Ag interface remains tight and defect-free (the enlarged view at this interface is not shown). The enlarged view at AISI 441 interface (Fig. 6a_2-6c_2) depicts that the oxide layer thickness only reaches ~ 15 μm after oxidation for 300 h, which is even thinner than that of the joints obtained by the traditional Ag-CuO braze without oxidation test (typically ≥ 20μm) [25, 32, 33]. Furthermore, the oxide layer in this study is much denser, and only a few micro-voids appeared after oxidation for 300 h. Both the thickness and compactness of the oxide layer indicate more superior oxidation resistance and aging performance of the joints fabricated by a pure Ag interlayer.

In brief, the above aging test demonstrates that YSZ/AISI 441 joints obtained with pure Ag interlayer present long-term (≥ 300 h) stability in both wet reducing atmosphere and oxidizing atmosphere. Due to the absence of CuO, the joints are more stable in a reducing atmosphere on the one hand, and the oxide layer formed on the stainless steel surface is much thinner and denser in the oxidizing atmosphere on the

other hand. Compared with the traditional RAB method, the method in this paper can greatly improve the service life of the joint, and it is more suitable for fabricating the SOFC/SOEC stacks.

4. Conclusions

In this study, the YSZ electrolyte is successfully joined to the AISI 441 interconnect using a pure Ag interlayer in air under an assembly pressure of ~ 2 MPa. The microstructure, mechanical properties, and aging properties of the joints are in-depth analyzed. The main conclusions can be summarized as follows:

(1) Dense and defect-free joints are fabricated at 920 ℃/30 min using the pure Ag interlayer. A thin and dense oxide layer (~ 2 μm) is observed at the Ag/AISI 441 interface. TEM results prove that the interatomic bonding of YSZ/Ag is achieved by forming a diffusion layer with disordered lattice (~ 3 nm) between them.

(2) No significant defects are observed at the YSZ/Ag interface at the temperature range of 860–950 ℃. This may be because Ag is soft enough to fill the gaps along the Ag/matrix interfaces under the pressure of ~ 2 MPa. The oxide layer at the AISI 441/Ag interface is thickened with the increasing temperature. The oxide layer thickness only reaches 2–3 μm even at 950°C, which is much thinner than traditional RAB joints (typically ≥ 20 μm).

(3) Lower temperatures will lead to insufficient diffusion of YSZ/Ag, resulting in poor bonding strength at the YSZ/Ag interface. In contrast, excessive temperatures can aggravate the oxidation at the AISI 441 interface, thus reducing the AISI 441/Ag interfacial strength. Therefore, the maximum shear strength of the joint (~ 86.1 MPa) is achieved at 920 ℃ in air, which is 161% higher than that of traditional RAB joints (~ 33 MPa).

(4) Aging tests demonstrate that YSZ/AISI 441 joints obtained with the pure Ag interlayer present superior long-term (≥ 300 h) stability in both reducing and oxidizing atmospheres. The joints are more stable in the reducing atmosphere due to the absence of CuO decomposition. Also, the oxide layer along the steel interconnect interface is much thinner and denser in the oxidizing atmosphere without the severe reactions between the CuO and steel.

This study presents that the YSZ/AISI 441 joints fabricated by the pure Ag interlayer possess enhanced mechanical and aging properties, which may improve the reliability and service life of SOFC/SOEC stacks.

Declarations

Author Statement

Xiaoqing Si: Methodology, Supervision, Validation, Conceptualization, Data curation, Writing-review & editing. **Xiaoyang Wang**: Investigation, Formal analysis, Validation, Visualization, Methodology, Data curation, Writing-original draft, Writing-review & editing. **Chun Li**: Methodology, Data curation, Writing-review & editing. **Tong Lin**: Writing-review & editing. **Junlei Qi**: Writing-review & editing. **Jian Cao***: Funding acquisition, Resources, Project administration, Supervision, Writing-review & editing.

Data availability statement

The raw/processed data required to reproduce these findings cannot be shared at this time as the data also forms part of an ongoing study.

Declaration of competing interest

The authors declare that they have no known competing financial interests or personal relationships that could have appeared to influence the work reported in this paper.

Acknowledgments

The authors gratefully acknowledge the financial support from the National Natural Science Foundation of China under Grant U1737205 and 52005131, the Postdoctoral Science Foundation of China 2019TQ0075, and the Heilongjiang Provincial Postdoctoral Science Foundation LBH-Z19142.

References

1. Singhal SC (2000) Advances in solid oxide fuel cell technology. Solid State Ionics 135:305–313. https://doi.org/10.1016/S0167-2738(00)00452-5
2. Xu N, Zhu T, Yang Z, Han M (2017) Fabrication and optimization of $La_{0.4}Sr_{0.6}Co_{0.2}Fe_{0.7}Nb_{0.1}O_{3-\delta}$ electrode for symmetric solid oxide fuel cell with zirconia based electrolyte. Journal of Materials Science Technology 33:1329–1333. https://doi.org/10.1016/j.jmst.2017.03.012
3. Sezer H, Mason JH, Celik IB, Yang T (2021) Three-dimensional modeling of performance degradation of planar SOFC with phosphine exposure. Int J Hydrogen Energy 46:6803–6816. https://doi.org/10.1016/j.ijhydene.2020.11.176
4. Si X, Cao J, Ritucci I, Talic B, Feng J, Kiebach R (2019) Enhancing the long-term stability of Ag based seals for solid oxide fuel/electrolysis applications by simple interconnect aluminization. Int J Hydrogen Energy 44:3063–3074. https://doi.org/10.1016/j.ijhydene.2018.11.071
5. Kong W, Zhang W, Huang H, Zhang Y, Wu J, Xu Y (2018) Analysis of micro-tubular SOFC stability under ambient and operating temperatures. Journal of Materials Science Technology 34:1436–1440. https://doi.org/10.1016/j.jmst.2017.12.009
6. Tucker MC (2010) Progress in metal-supported solid oxide fuel cells: A review. Journal of Power Sources 195:4570–4582. https://doi.org/10.1016/j.jpowsour.2010.02.035

7. Wang Z, Li C, Si X, Yang B, Huang Y, Qi J, Feng J, Cao J (2020) Brazing YSZ ceramics by a novel SiO_2 nanoparticles modified Ag filler. Ceram Int 46:16493–16501. https://doi.org/10.1016/j.ceramint.2020.03.214
8. Han M, Tang X, Yin H, Peng S (2007) Fabrication, microstructure and properties of a YSZ electrolyte for SOFCs. Journal of Power Sources 165:757–763. https://doi.org/10.1016/j.jpowsour.2006.11.054
9. Wang Y, Li W, Ma L, Li W, Liu X (2020) Degradation of solid oxide electrolysis cells: Phenomena, mechanisms, and emerging mitigation strategies–A review. Journal of Materials Science Technology 55:35–55. https://doi.org/10.1016/j.jmst.2019.07.026
10. Blum L, Meulenberg WA, Nabielek H, Steinberger-Wilckens R (2005) Worldwide SOFC Technology Overview and Benchmark. Int J Applied Ceramic Technology 2:482–492. https://doi.org/10.1111/j.1744-7402.2005.02049.x
11. Jeon SK, Nahm SH, Kwon OH (2015) Improvement in the Adhesion Between Electrode of a SOFC and Ag Paste as a Current Collector by Au Deposition. Journal of Materials Science Technology 31:257–263. https://doi.org/10.1016/j.jmst.2014.09.015
12. Ferraris M, De la Pierre S, Sabato AG, Smeacetto F, Javed H, Walter C, Malzbender J (2020) Torsional shear strength behavior of advanced glass-ceramic sealants for SOFC/SOEC applications. Journal of the European Ceramic Society 40:4067–4075. https://doi.org/10.1016/j.jeurceramsoc.2020.04.034
13. Wu J, Liu X, Recent Development of SOFC Metallic Interconnect, J. Mater. Sci. Technol. (2010) 13
14. Mahmud LS, Muchtar A, Somalu MR (2017) Challenges in fabricating planar solid oxide fuel cells: A review. Renewable Sustainable Energy Reviews 72:105–116. https://doi.org/10.1016/j.rser.2017.01.019
15. Kiebach R, Engelbrecht K, Grahl-Madsen L, Sieborg B, Chen M, Hjelm J, Norrman K, Chatzichristodoulou C, Hendriksen PV (2016) An Ag based brazing system with a tunable thermal expansion for the use as sealant for solid oxide cells. Journal of Power Sources 315:339–350. https://doi.org/10.1016/j.jpowsour.2016.03.030
16. Zhu WZ, Deevi SC (2003) Development of interconnect materials for solid oxide fuel cells. Materials Science Engineering: A 348:227–243. https://doi.org/10.1016/S0921-5093(02)00736-0
17. Si X, Cao J, Talic B, Ritucci I, Li C, Qi J, Feng J, Kiebach R (2020) A novel Ag based sealant for solid oxide cells with a fully tunable thermal expansion. Journal of Alloys Compounds 831:154608. https://doi.org/10.1016/j.jallcom.2020.154608
18. Si X, Cao J, Song X, Qu Y, Feng J (2017) Reactive air brazing of YSZ ceramic with novel Al_2O_3 nanoparticles reinforced Ag-CuO-Al_2O_3 composite filler: Microstructure and joint properties. Materials Design 114:176–184. https://doi.org/10.1016/j.matdes.2016.10.062
19. Si X, Cao J, Song X, Wang Z, Wang Z, Feng J (2017) Evolution behavior of Al_2O_3 nanoparticles reinforcements during reactive air brazing and its role in improving the joint strength. Materials Design 132:96–104. https://doi.org/10.1016/j.matdes.2017.07.002

20. Zhao BT,Y, Thermo-Mechanical Properties of Glass-Ceramic Solid Oxide Fuel Cell Sealant Materials, (2013) 141
21. Smeacetto F, Chrysanthou A, Salvo M, Zhang Z, Ferraris M (2009) Performance and testing of glass-ceramic sealant used to join anode-supported-electrolyte to Crofer22APU in planar solid oxide fuel cells. Journal of Power Sources 190:402–407. https://doi.org/10.1016/j.jpowsour.2009.01.042
22. Chang H-T, Lin C-K, Liu C-K (2010) Effects of crystallization on the high-temperature mechanical properties of a glass sealant for solid oxide fuel cell. Journal of Power Sources 195:3159–3165. https://doi.org/10.1016/j.jpowsour.2009.12.008
23. Reis ST, Pascual MJ, Brow RK, Ray CS, Zhang T (2010) Crystallization and processing of SOFC sealing glasses. J Non-Cryst Solids 356:3009–3012. https://doi.org/10.1016/j.jnoncrysol.2010.02.028
24. Bobzin K, Öte M, Wiesner S, Kaletsch A, Broeckmann C (2014) Characterization of Reactive Air Brazed Ceramic/Metal Joints with Unadapted Thermal Expansion Behavior: RAB Joints with Unadapted Thermal Expansion Behavior. Adv Eng Mater 16:1490–1497. https://doi.org/10.1002/adem.201400311
25. Cao J, Wang Z, Li C, Si X, Yang B, Guo X, Huang Y, Qi J (2021) Microstructure evolution and mechanical properties of Co coated AISI 441 ferritic stainless steel/ YSZ reactive air brazed joint. Int J Hydrogen Energy 46:8758–8766. https://doi.org/10.1016/j.ijhydene.2020.12.059
26. Raju K, Muksin S, Kim K, Song JH, Yu D-H, Yoon, Joining of metal-ceramic using reactive air brazing for oxygen transport membrane applications, Materials & Design. 109 (2016) 233–241. https://doi.org/10.1016/j.matdes.2016.07.068
27. Luo Y, Song XG, Hu SP, Xu ZQ, Li ZH, Lei Y (2021) Reactive air brazing of Al_2O_3 ceramic with Ag-CuO-Pt composite fillers: Microstructure and joint properties. Journal of the European Ceramic Society 41:1407–1414. https://doi.org/10.1016/j.jeurceramsoc.2020.10.008
28. Weil KS, Kim JY, Hardy JS (2005) Reactive Air Brazing: A Novel Method of Sealing SOFCs and Other Solid-State Electrochemical Devices, Electrochem. Solid-State Lett 8:A133. https://doi.org/10.1149/1.1850391
29. Kaletsch A (2012) Effects of Copper Oxide Content in AgCuO Braze Alloy on Microstructure and Mechanical Properties of Reactive-Air-Brazed $Ba_{0.5}Sr_{0.5}Co_{0.8}Fe_{0.2}O_{3-\delta}$ (BSCF). J Ceram Sci Tech. https://doi.org/10.4416/JCST2012-00001
30. Chatzimichail R, Triantafyllou G, Tietz F, Nikolopoulos P (2014) Interfacial properties of (Ag + CuO) brazes used as sealing materials in SOFC stacks. J Mater Sci 49:300–313. https://doi.org/10.1007/s10853-013-7706-x
31. Kim J, Hardy J, Weil S (2007) Dual-atmosphere tolerance of Ag–CuO-based air braze. Int J Hydrogen Energy 32:3655–3663. https://doi.org/10.1016/j.ijhydene.2006.08.054
32. Kuhn B, Wetzel FJ, Malzbender J, Steinbrech RW, Singheiser L (2009) Mechanical performance of reactive-air-brazed (RAB) ceramic/metal joints for solid oxide fuel cells at ambient temperature. Journal of Power Sources 193:199–202. https://doi.org/10.1016/j.jpowsour.2008.10.117

33. Kuhn B, Wessel E, Malzbender J, Steinbrech RW, Singheiser L (2010) Effect of isothermal aging on the mechanical performance of brazed ceramic/metal joints for planar SOFC-stacks. Int J Hydrogen Energy 35:9158–9165. https://doi.org/10.1016/j.ijhydene.2010.06.063
34. Zhou Q, Bieler TR, Nicholas JD (2018) Transient porous nickel interlayers for improved silver-based Solid Oxide Fuel Cell brazes. Acta Mater 148:156–162. https://doi.org/10.1016/j.actamat.2018.01.061
35. Phongpreecha T, Nicholas JD, Bieler TR, Qi Y (2018) Computational design of metal oxides to enhance the wetting and adhesion of silver-based brazes on yttria-stabilized-zirconia. Acta Mater 152:229–238. https://doi.org/10.1016/j.actamat.2018.04.024
36. Pönicke A, Schilm J, Kusnezoff M, Michaelis A, Aging Behavior of Reactive Air Brazed Seals for SOFC, Fuel Cells. 15 (2015) 735–741. https://doi.org/10.1002/fuce.201400192
37. Scott Weil K, Coyle CA, Darsell JT, Xia GG, Hardy JS (2005) Effects of thermal cycling and thermal aging on the hermeticity and strength of silver–copper oxide air-brazed seals. J Power Sources 152:97–104. https://doi.org/10.1016/j.jpowsour.2005.01.053
38. Zeng Z, Qian Y, Zhang Y, Hao C, Dan D, Zhuge W, A review of heat transfer and thermal management methods for temperature gradient reduction in solid oxide fuel cell (SOFC) stacks, Applied Energy. 280 (2020) 115899. https://doi.org/10.1016/j.apenergy.2020.115899
39. Ding J, Zhou X, Liu Q, Yin G (2018) Development of tubular anode-supported solid oxide fuel cell cell and 4-cell-stack based on lanthanum gallate electrolyte membrane for mobile application. Journal of Power Sources 401:336–342. https://doi.org/10.1016/j.jpowsour.2018.08.089
40. Wang Z, Li C, Si X, Liu Y, Qi J, Huang Y, Feng J, Cao J (2020) Oxidation behavior of ferritic stainless steel interconnect coated by a simple diffusion bonded cobalt protective layer for solid oxide fuel cells. Corros Sci 172:108739. https://doi.org/10.1016/j.corsci.2020.108739
41. Alnegren P, Sattari M, Svensson J-E, Froitzheim J (2018) Temperature dependence of corrosion of ferritic stainless steel in dual atmosphere at 600–800°C. Journal of Power Sources 392:129–138. https://doi.org/10.1016/j.jpowsour.2018.04.088
42. Gunduz KO, Chyrkin A, Goebel C, Hansen L, Hjorth O, Svensson J-E, Froitzheim J (2021) The effect of hydrogen on the breakdown of the protective oxide scale in solid oxide fuel cell interconnects. Corros Sci 179:109112. https://doi.org/10.1016/j.corsci.2020.109112
43. Si X, Cao J, Kiebach R, Xu Y, Xu H, Talic B, Feng J (2018) Joining of solid oxide fuel/electrolysis cells at low temperature: A novel method to obtain high strength seals already at 300°C. Journal of Power Sources 400:296–304. https://doi.org/10.1016/j.jpowsour.2018.08.046
44. Hu G, Zhou Q, Bhatlawande A, Park J, Termuhlen R, Ma Y, Bieler TR, Yu H-C, Qi Y, Hogan T, Nicholas JD (2021) Patterned nickel interlayers for enhanced silver wetting, spreading and adhesion on ceramic substrates. Scripta Mater 196:113767. https://doi.org/10.1016/j.scriptamat.2021.113767

Figures

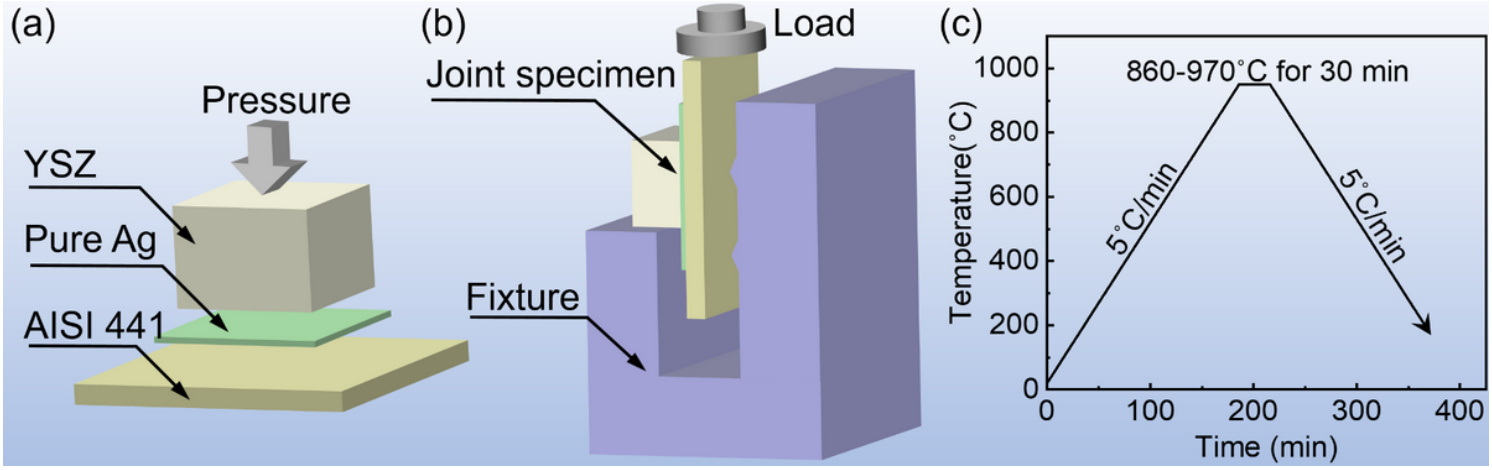

Figure 1

(a) Schematic diagram of joining assembly, (b) sketch of the shear test, and (c) joining temperature curve.

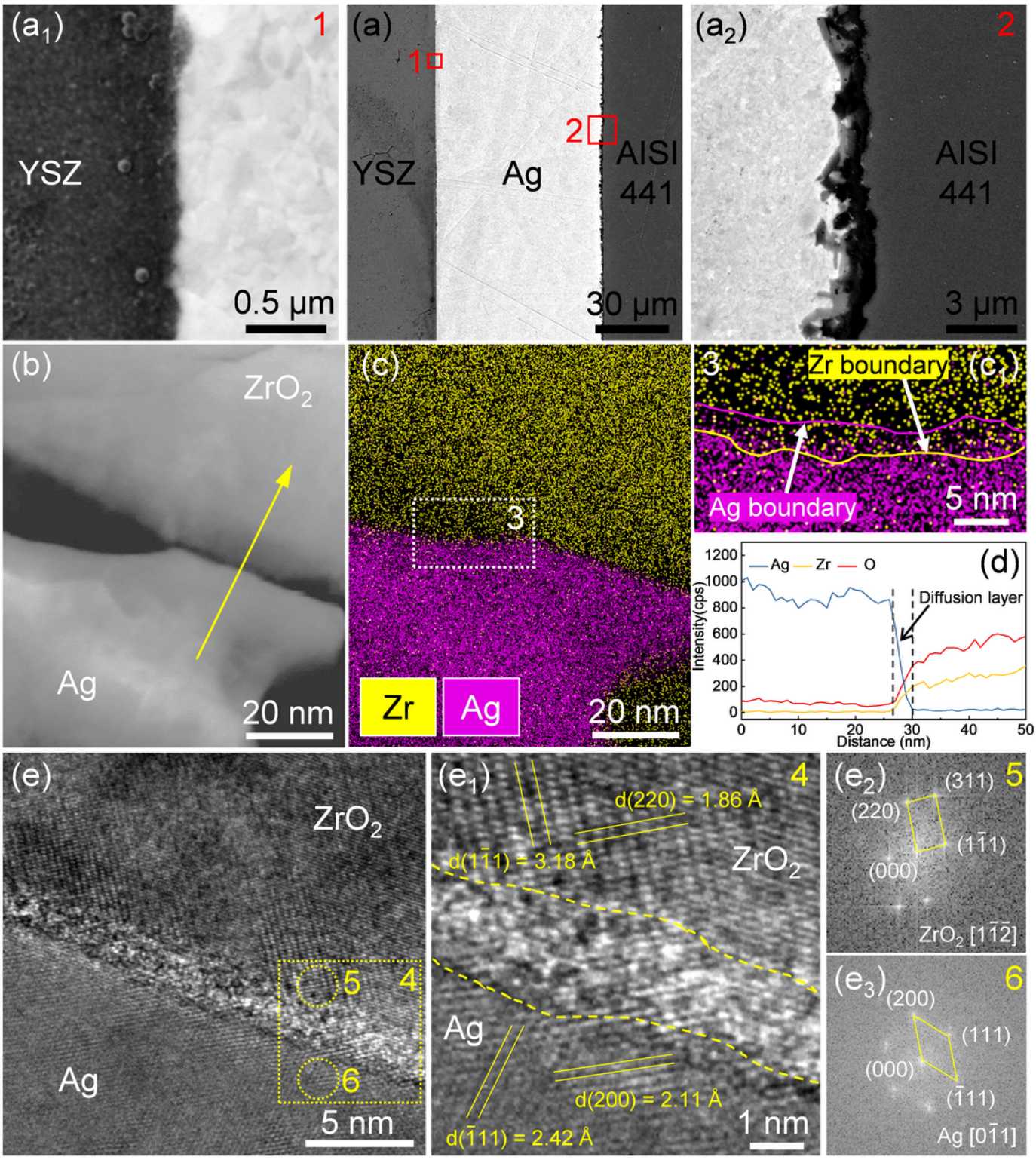

Figure 2

(a) Microstructure of YSZ/AISI 441 joint obtained using Ag interlayer at 920°C/30 min, enlarged SEM image of (a1) YSZ interface and (a2) AISI 441interface; (b) bright-field image at the YSZ/Ag interface, (c) corresponding EDS mapping results, (c1) enlarged view of region 3, (d) elemental distributions of Ag, Zr, and O along the yellow line, (e) HRTEM image at YSZ/Ag interface, (e1) enlarged view of region 4, corresponding Fast Fourier Transformation of (e2) region 5 and (e3) region 6.

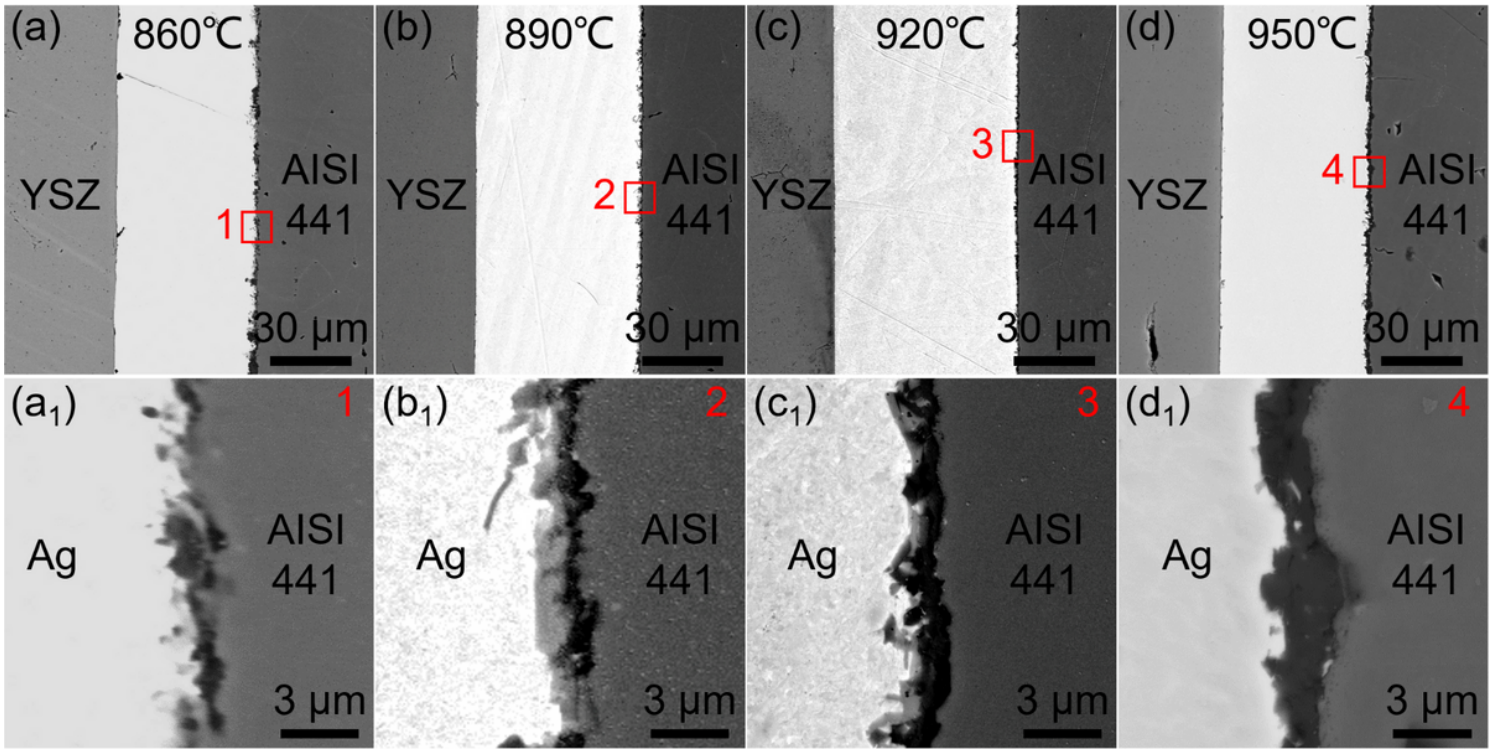

Figure 3

Interfacial microstructure of YSZ/AISI 441 joints obtained at various bonding temperatures for 30 min: (a) 890 °C, (b) 910 °C, (c) 930 °C, and (d) 950 °C; (a1)-(d1) corresponding enlarged view at the Ag/AISI 441 interface.

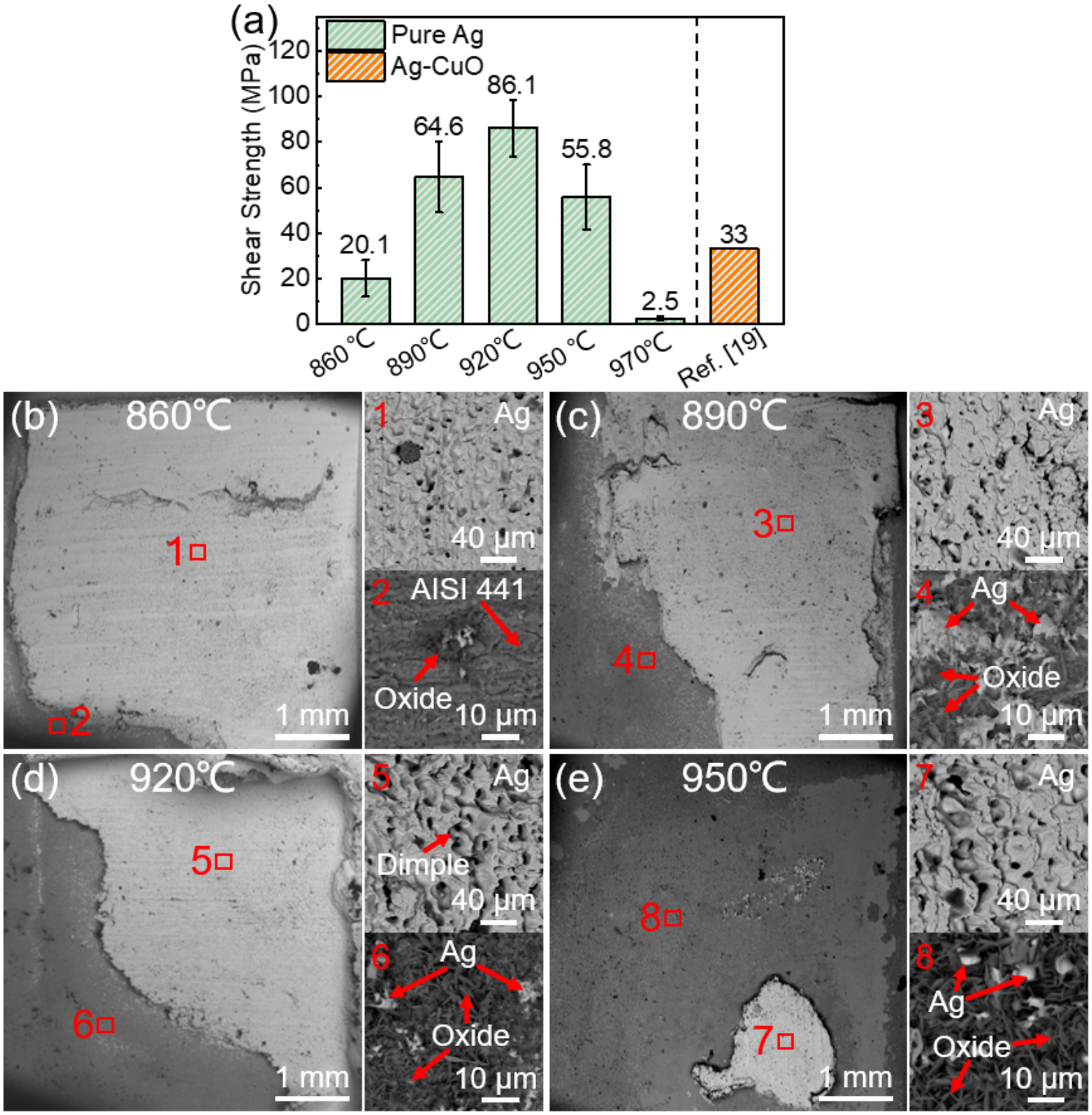

Figure 4

(a) Room-temperature shear strength of the joints obtained at various conditions using Ag interlayer and Ag-CuO braze; corresponding fracture surfaces at various joining temperatures at AISI 441 side: (b) 860°C, (c) 890°C, (d) 920°C, and (e) 950°C.

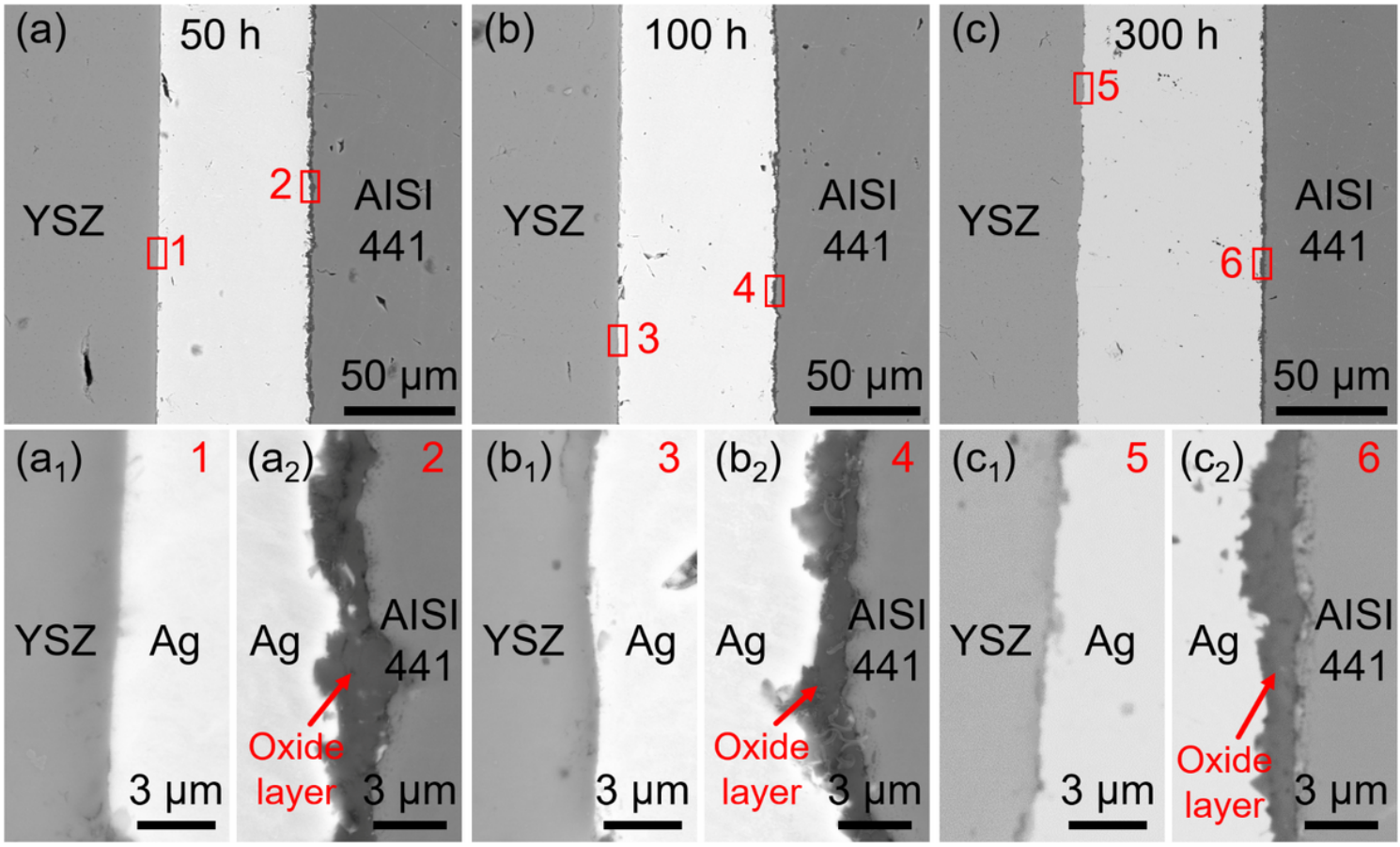

Figure 5

Interfacial microstructure of the joints obtained using the pure Ag interlayer after aging in 50% (H2+Ar)-50% H2O at 800 ℃ for (a) 50 h, (b) 100 h, and (c) 300 h, respectively. (a1, b1, and c1 are the corresponding enlarged views of the YSZ interface, a2, b2, and c2 are the corresponding enlarged views of the AISI 441 interface)

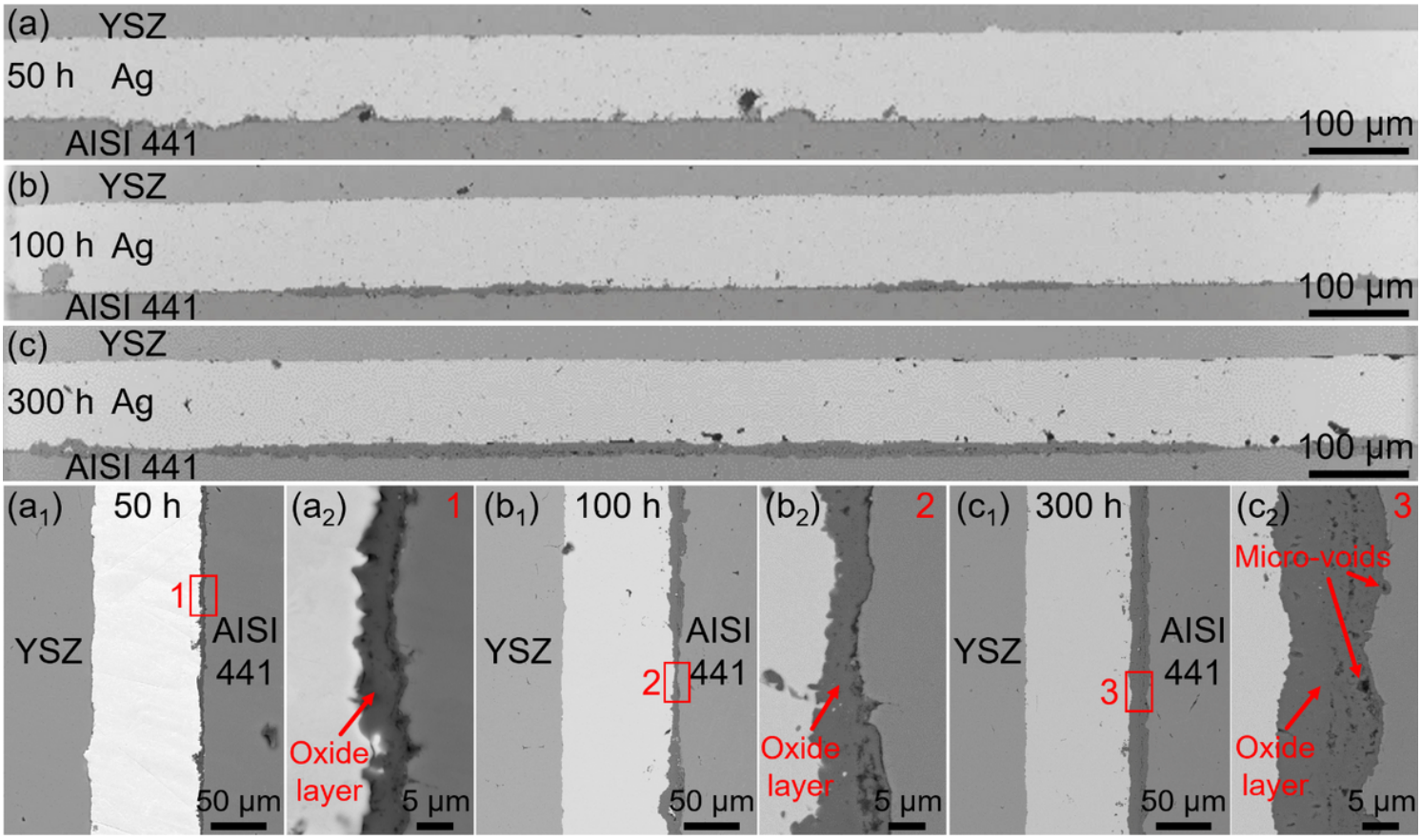

Figure 6

Overview SEM image of the joints in low magnification after aging in air at 800 °C for (a) 50 h, (b) 100 h, and (c) 300 h, respectively. (a1, b1, and c1 are the corresponding interfacial microstructure of joints, a2, b2, and c2 are the corresponding enlarged views at the AISI 441 interface)

Supplementary Files

This is a list of supplementary files associated with this preprint. Click to download.

- supplementarymaterial.docx